Available online at www.sciencedirect.com

ScienceDirect

IFAC Papers Online CONFERENCE PAPER ARCHIVE

IFAC PapersOnLine 54-19 (2021) 294–301

A Direct Bounded Control Method for Transient Stability Assessment ⋆

Jianli Gao * **Balarko Chaudhuri** * **Alessandro Astolfi** *,**

* *Department of Electrical and Electronic Engineering, Imperial College London, London, SW7 2AZ, UK. (e-mail: jianli.gao18@imperial.ac.uk, b.chaudhuri@imperial.ac.uk)*

** *Dipartimento di Ingegneria Civile e Ingegneria Informatica, Università di Roma "Tor Vergata", 00133 Roma, Italy. (e-mail: a.astolfi@imperial.ac.uk)*

Abstract: The paper proposes a direct method for transient stability assessment, which is more efficient than traditional time-domain simulation methods. To achieve this objective, a new bounded control law for the model of a power system is designed. This yields superior closed-loop transient performances when compared to those achievable with traditional automatic voltage regulators and power system stabilizers. The designed control law allows defining an energy-based Lyapunov function which is instrumental in assessing transient stability properties of the post-fault system. A case study on a single machine infinite bus power system model is presented to illustrate the merits of the proposed method.

Copyright © 2021 The Authors. This is an open access article under the CC BY-NC-ND license (https://creativecommons.org/licenses/by-nc-nd/4.0/)

Keywords: Transient stability, power systems, bounded control, Lyapunov function

1. INTRODUCTION

The assessment of transient stability for power systems is a long-standing challenging problem because of their intrinsic complex characteristics, such as switching actions, highly non-linear behaviours, non-measurable states and control bounds, see *e.g.* Kundur et al. (1994); Sauer and Pai (1998); Guo et al. (2001); Liberzon (2003); Ortega et al. (2005); Hatziargyriou et al. (2020). Currently, time-domain simulations (TDS) offer one of the most widely accepted methods for the assessment of transient stability of a post-fault power system, see *e.g.* Kundur et al. (1994); Chiang (2011). In TDS methods the numerical integration of a model of the power system is conducted to simulate the transient response. Based on the simulation, the post-fault system is assessed to be stable if the post-fault trajectory converges to an operating equilibrium; otherwise, it is deemed to be unstable and then corrective actions have to be undertaken, see *e.g.* Chiang (2011). This off-line practice is computationally expensive and therefore not well-suited for real-time implementations, see *e.g.* Chiang (2011); Yan et al. (2011). Compared to TDS methods, direct methods have a distinct advantage in that they allow assessing transient stability of a post-fault trajectory without time-consuming numerical integrations, see *e.g.* Kundur et al. (1994); Chiang (2011). Therefore, direct methods offer a promising solution to the problem of real-time transient stability analysis, see *e.g.* Chiang (2011).

Transient stability can be assessed by checking that the post-fault trajectory, at the instant the fault is cleared, belongs to the region of attraction of the post-fault operating equilibrium. As a result, it is natural to expect that Lyapunov or energy functions play a dominant role in the development of direct methods, see *e.g.* Chiang (2011). For example, in Pai and Sauer (1989); Bretas and Alberto (2003), energy-based Lyapunov functions have been proposed for transient stability analysis. These are, however, valid only for second order models of generators which neglect the dynamics associated with the flux linkage through the generator field and damper windings. When extended to the study of third order or higher order models, Lyapunov or energy functions become more complex. In Ortega et al. (2005), the proposed control law endows the third order model of a generator with a port-controlled Hamiltonian structure, for which a separable Lyapunov function can be employed in transient stability analysis. In Ghandhari et al. (2001), another form of energy-based control Lyapunov function for the third order model of a generator is proposed. In Jiang and Chiang (2015), a fifth order model including the stator transient dynamics has been used in the study of transient stability over two timescales, however, without the use of Lyapunov or energy functions. In Verrelli et al. (2021), the generator model studied includes the dynamic of the electric power output; however, it does not consider the dynamic of the induced voltage nor proposes a Lyapunov or energy function.

Control bounds are of great importance in power systems due to the physical limitations of thyristor excitation systems, see *e.g.* Kundur et al. (1994). However, in all the studies discussed above, the control bounds are not taken into consideration in the design stage. In the

⋆ This work has been partially supported by the European Union's Horizon 2020 Research and Innovation Programme under grant agreement No 739551 (KIOS CoE), and by the Italian Ministry for Research in the framework of the 2017 Program for Research Projects of National Interest (PRIN), Grant no. 2017YKXYXJ.

2405-8963 Copyright © 2021 The Authors. This is an open access article under the CC BY-NC-ND license.
Peer review under responsibility of International Federation of Automatic Control.
10.1016/j.ifacol.2021.11.093

transient stability study for power systems controlled with traditional automatic voltage regulators (AVR) and power system stablizers (PSS), see *e.g.* Kundur et al. (1994), the control bounds are taken into account in the implementation stage. This is achieved by forcing the control input to stay at the boundaries when it is about to exceed the feasible range. However, there exists no Lyapunov or energy function such that its time derivative along the trajectories of the closed-loop system is strictly negative definite. It is therefore difficult to assess, through direct methods, the transient stability properties of the post-fault system controlled with AVR and PSS.

This paper addresses some of the above-mentioned issues. In particular it focuses on, firstly, the design of a control law for the third order model of a generator which takes into account the control bounds. This is achieved through the use of symmetric and asymmetric saturation functions in the design stage. Then, exploiting the proposed bounded control law, an energy-based Lyapunov function is proposed to assess local stability of the closed-loop operating equilibrium as well as transient stability of the post-fault trajectories.

The remaining of the paper is organized as follows. In Section 2 the classical third order model for the single machine infinite bus (SMIB) system is recalled. Then, the problem of transient stability analysis of the post-fault SMIB power system is formulated. In Section 3 a new bounded control law is designed, based on which local stability of the closed-loop operating equilibrium is proved through a Lyapunov approach. Then, an algorithm for transient stability assessment of post-fault trajectories is introduced. In Section 4 a case study to demonstrate the merits of the designed control law as well as of the direct method is presented. Finally, conclusions are drawn and potential future work is discussed in Section 5.

2. MODELLING AND PROBLEM FORMULATION

The system studied consists of a synchronous generator (SG) connected to an infinite bus through a transformer and two parallel transmission lines, as illustrated in Fig. 1. This is henceforth referred to as the SMIB power system. Note that the SG terminal bus, the bus at the sending end of the transmission lines and the infinite bus are henceforth referred to as bus 1, bus 2 and bus 3, respectively.

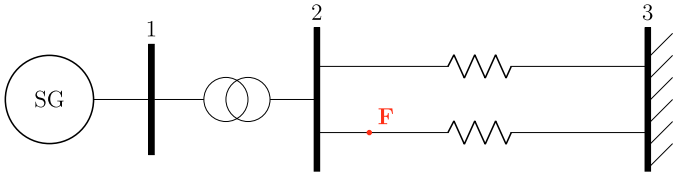

Fig. 1. Single machine infinite bus (SMIB) power system, from Kundur et al. (1994). Note that **F** represents the location where the fault occurs in the case study.

A simplified dynamic model of the SG which neglects the dynamics of the induced voltage due to the change in flux linkage in both the d-axis and the q-axis damper windings is considered. The resulting third order model describing the dynamics of the generator rotor angle $\delta(t) \in [0, \pi]$, of the rotational speed $\omega(t) \in \mathbb{R}_{\geq 0}$, and of the induced voltage $E'_q(t) \in \mathbb{R}_{\geq 0}$ due to the change in flux linkage in the generator field winding is given by the equations

$$\dot{\delta} = \omega - \omega^*, \tag{1}$$

$$\dot{\omega} = -\frac{D}{2H}(\omega - \omega^*) + \frac{\omega^*}{2H}(P_m - P_e), \tag{2}$$

$$\dot{E}'_q = \frac{1}{T'_{d0}}\big[- E'_q + (X_d - X'_d)I_d + E_{fd}\big], \tag{3}$$

where ω^* is the constant synchronous speed, D is the damping constant, H is the inertia constant, P_m is the mechanical power input to the SG (assumed to be constant over the timescale of the transient stability analysis), P_e is the electrical power output from the SG, T'_{d0} is the q-axis open circuit time constant, X_d is the d-axis synchronous reactance, X'_d is the d-axis transient reactance, I_d is the d-axis component of the stator current, and E_{fd} is the bounded field voltage.

The electrical power output $P_e \in \mathbb{R}_{\geq 0}$ and the electrical torque output $T_e \in \mathbb{R}_{\geq 0}$ from the SG are given by

$$P_e = \frac{T_e\,\omega}{\omega^*}, \tag{4}$$

$$T_e = E'_q\, I_q + E'_d\, I_d - (X'_q - X'_d) I_d\, I_q, \tag{5}$$

respectively, where I_q is the q-axis component of the stator current, E'_d is the induced voltage due to the change in flux linkage in the q-axis damper winding (assumed to be constant), and X'_q is the q-axis transient reactance.

The SG stator transients are much faster compared to the slow electro-mechanical dynamics and hence are neglected, see *e.g.* Chaudhuri et al. (2014); Hatziargyriou et al. (2020). The complex stator current $\bar{I}_g$ in the d-q reference frame of the SG is given by

$$\bar{I}_g = \frac{[E'_q + j(E'_d - (X'_q - X'_d)I_q)] - \bar{E}_t e^{-j\delta}}{R_a + jX'_d}, \tag{6}$$

where $\bar{E}_t$ is the voltage of bus 1 expressed in a common network D-Q reference frame and R_a is the stator resistance.

In the studied model of the SG, the d/D-axis leads the q/Q-axis by 90 degrees as illustrated in Fig. 2. Note that the generator rotor angle δ is defined as the angular separation between the q-axis and the Q-axis, see *e.g.* Chaudhuri et al. (2014).

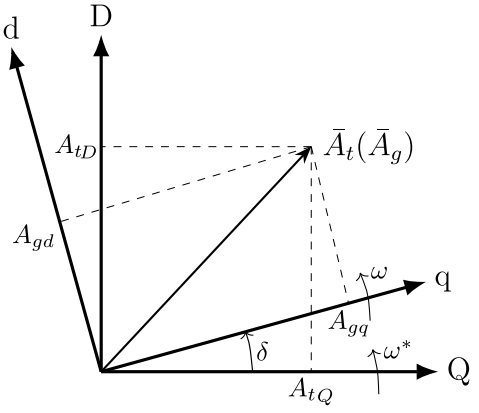

Fig. 2. The d-q and D-Q reference frames, from Chaudhuri et al. (2014)

A complex quantity $\bar{A}_g$, *e.g.* a voltage or a current, expressed in the generator d-q reference frame is related to the same quantity $\bar{A}_t$ expressed in the network D-Q reference frame by the equation

$$\bar{A}_t = (A_{tQ} + jA_{tD}) = \bar{A}_g e^{j\delta} = (A_{gq} + jA_{gd})e^{j\delta}. \quad (7)$$

The complex current $\bar{I}_t$ injected by the SG into the network at bus 1 is given by

$$\bar{I}_t = \bar{I}_g e^{j\delta} = (I_q + jI_d)e^{j\delta}. \quad (8)$$

Applying current balance, *i.e. Kirchoff's current law*, at bus 1 yields

$$\bar{I}_t = \bar{Y}_{11}\bar{E}_t + \bar{Y}_{13}\bar{E}_B, \quad (9)$$

where $\bar{Y}_{11}$ and $\bar{Y}_{13}$ are the diagonal and the off-diagonal elements corresponding to bus 1 of the bus admittance matrix for the SMIB power system after eliminating bus 2, and $\bar{E}_B$ is the voltage of bus 3.

Solving (6), (8) and (9) by equating the real and imaginary parts, respectively, yields the components of the stator current, *i.e.* $I_d(\delta, E'_q)$ and $I_q(\delta, E'_q)$. Then, substituting these in (2), (3), (4) and (5) yields the dynamic equations

$$\dot{\delta} = \omega - \omega^*, \quad (10)$$

$$\dot{\omega} = -\frac{D + T_e}{2H}(\omega - \omega^*) + \frac{\omega^*}{2H}(P_m - T_e), \quad (11)$$

$$\dot{E}'_q = -a_\epsilon E'_q + b_\epsilon \cos\delta + e_f + u, \quad (12)$$

where e_f is the constant field voltage, u is the control input, and the electrical torque output $T_e \in \mathbb{R}_{\geq 0}$ is

$$T_e = a_\tau {E'_q}^2 + b_\tau \sin\delta\, E'_q + c_\tau \sin 2\delta + d_\tau \cos\delta. \quad (13)$$

Note that the electrical torque output at the operating equilibrium point $(\delta^*, {E'_q}^*)$ is equal to the mechanical power input, *i.e.*

$$T_e(\delta^*, {E'_q}^*) = P_m. \quad (14)$$

It is assumed that a fault occurs at the location **F** shown in Fig. 1. This results in the switching from the pre-fault mode to the fault-on mode. Then, the fault is cleared by disconnecting the faulted transmission line, resulting in the switching from the fault-on mode to the post-fault mode.

As indicated in Kundur et al. (1994), the values of the coefficients in the pre-fault mode, the fault-on mode and the post-fault mode, respectively, are given in Table 1. The operating equilibria for the pre-fault mode and the post-fault mode are also given in Table 1. Note that there exists no operating equilibrium in the fault-on mode.

Table 1. Coefficients in different modes

Mode	Pre-fault	Fault-on	Post-fault
a_ϵ	0.3251	0.4698	0.0050
b_ϵ	0.1803	0	0.1471
a_τ	0.0050	0.0148	0.0033
b_τ	1.1621	0	0.9482
c_τ	-0.1628	0	-0.1150
d_τ	-0.2853	0	-0.2469
δ^*	1.1567	-	1.3549
${E'_q}^*$	1.0483	-	1.0598

In addition, the values of the constant parameters of the considered SMIB power system are given in Table 2. Throughout the paper we use these parameters for ease of illustration, although the conclusions are general.

Table 2. Constant parameters of the SMIB power system model

D	H	P_m	ω^*	e_f
0	3.5	0.8829	120π	0.2677

With the aforementioned specifications, the problem of transient stability assessment is formulated as follows. Consider the model of a SMIB power system, *i.e.* (10), (11), (12) and (13). Find a state feedback control law such that the following specifications are satisfied.

- The control input remains within its physical bounds. For the considered case, these are $u_{max} = 0.6073$ and $u_{min} = -1.0677$, respectively.
- The operating equilibrium of the post-fault closed-loop SMIB power system is preserved and it is locally asymptotically stable.
- There exists an energy-based Lyapunov function which allows assessing transient stability of the post-fault trajectory.

3. BOUNDED CONTROL DESIGN

To begin with, consider the second order mechanical subsystem, namely the system

$$\dot{\delta} = \omega - \omega^*, \quad (15)$$

$$\dot{\omega} = -\frac{D + \tilde{T}_e}{2H}(\omega - \omega^*) + \frac{\omega^*}{2H}(P_m - \tilde{T}_e), \quad (16)$$

where

$$\tilde{T}_e = a_\tau {\tilde{E}'_q}^2 + b_\tau \sin\delta\, \tilde{E}'_q + c_\tau \sin 2\delta + d_\tau \cos\delta. \quad (17)$$

Note that, at this stage, the term $\tilde{E}'_q$ is regarded as a control input. Let

$$\tilde{E}'_q = {E'_q}^* + \mathrm{sat}(\omega - \omega^*), \quad (18)$$

where [1]

$$\mathrm{sat}(\omega - \omega^*) = L_\tau \tanh\Big(\frac{k_\tau}{L_\tau}(\omega - \omega^*)\Big), \quad (19)$$

with $L_\tau \in \mathbb{R}_{>0}$ the magnitude of the saturation, and $k_\tau \in \mathbb{R}_{>0}$ the slope of the saturation at the equilibrium, both to be selected.

To prove stability of the operating equilibrium of the closed-loop second order subsystem, a Lyapunov approach is used. Let $\tilde{D}_\tau = (D + \tilde{T}_e)/(2H)$. Since $\tilde{T}_e$ is non-negative and $D = 0$, $\tilde{D}_\tau$ is non-negative. Then, (16) can be rewritten as

$$\begin{aligned}\dot{\omega} &= -\tilde{D}_\tau(\omega - \omega^*) + \frac{\omega^*}{2H}\Big(P_m - a_\tau\big[{E'_q}^* + \mathrm{sat}(\omega - \omega^*)\big]^2 \\ &\quad - b_\tau \sin\delta\,\big[{E'_q}^* + \mathrm{sat}(\omega - \omega^*)\big] - c_\tau \sin 2\delta - d_\tau \cos\delta\Big) \\ &= -\tilde{D}_\tau(\omega - \omega^*) - \tilde{\gamma}(\delta) - \tilde{d}\,\mathrm{sat}(\omega - \omega^*), \quad (20)\end{aligned}$$

where

$$\begin{aligned}\tilde{\gamma}(\delta) = \frac{\omega^*}{2H}\Big(&- P_m + a_\tau {E'_q}^{*2} + b_\tau \sin\delta\, {E'_q}^* \\ &+ c_\tau \sin 2\delta + d_\tau \cos\delta\Big),\end{aligned}$$

$$\tilde{d} = \frac{\omega^*}{2H}\Big(2a_\tau {E'_q}^* + a_\tau\,\mathrm{sat}(\omega - \omega^*) + b_\tau \sin\delta\Big).$$

[1] Note that any differentiable, monotonically increasing saturation function can be used.

Note that $\tilde{\gamma}(\delta^*) = 0$, $\frac{d\tilde{\gamma}}{d\delta}(\delta^*) > 0$, and $\tilde{d}$ is locally positive around the operating equilibrium.

Consider the Lyapunov function candidate

$$\tilde{V}(\delta,\omega) = \frac{1}{2}(\omega-\omega^*)^2 + \int_{\delta^*}^{\delta} \tilde{\gamma}(\xi)\, d\xi + \tilde{c}, \tag{21}$$

where $\tilde{c}$ is such that $\tilde{V}(\delta^*,\omega^*) = 0$. Note that $\tilde{V}$ is locally positive definite around the operating equilibrium. Taking the time-derivative of $\tilde{V}$ along the trajectories of the closed-loop system (15), (16), (17), (18) and (19) yields

$$\begin{aligned}\dot{\tilde{V}} &= (\omega-\omega^*)\,\dot{\omega} + \tilde{\gamma}(\delta)\,\dot{\delta}\\ &= -\tilde{D}_\tau\,(\omega-\omega^*)^2 - \tilde{d}\,(\omega-\omega^*)\,\mathrm{sat}(\omega-\omega^*)\\ &\le -\tilde{D}_\tau\,(\omega-\omega^*)\,\mathrm{sat}(\omega-\omega^*) - \tilde{d}\,(\omega-\omega^*)\,\mathrm{sat}(\omega-\omega^*)\\ &= -\left(\tilde{D}_\tau + \tilde{d}\right)(\omega-\omega^*)\,\mathrm{sat}(\omega-\omega^*) \le 0,\end{aligned} \tag{22}$$

from which we conclude local stability of the operating equilibrium of the second order closed-loop system.

Consider now the third order model, *i.e.* (10), (11), (12) and (13). For such a model the excitation control is designed so that the closed-loop dynamics of the state E'_q "tracks" the state-dependent reference $\tilde{E}'_q$ given in (18). This objective can be achieved by using the bounded state feedback control law

$$\begin{aligned}u(\delta,\omega,E'_q) = a_\epsilon \tilde{E}'_q - b_\epsilon\cos\delta - e_f - \mathrm{Sat}\big(E'_q - \tilde{E}'_q\big)\\ + k_\tau\left(1 - \frac{sat^2(\omega-\omega^*)}{{L_\tau}^2}\right)\dot{\omega},\end{aligned} \tag{23}$$

where $\mathrm{Sat}\big(E'_q - \tilde{E}'_q\big)$ is a differentiable saturation function with adjustable bounds defined as

$$\mathrm{Sat}(\varepsilon) = \begin{cases} L_u^+ \tanh\left(\dfrac{k_u}{L_u^+}\varepsilon\right), & \varepsilon > 0,\\ 0, & \varepsilon = 0,\\ L_u^- \tanh\left(\dfrac{k_u}{L_u^-}\varepsilon\right), & \varepsilon < 0,\end{cases} \tag{24}$$

with $\varepsilon = E'_q - \tilde{E}'_q \in \mathbb{R}$, $k_u \in \mathbb{R}_{>0}$, and $L_u^+ \in \mathbb{R}_{\ge 0}$ and $L_u^- \in \mathbb{R}_{\ge 0}$ the magnitudes of the positive bound and of the negative bound, respectively.

Note that L_u^+ and L_u^- are functions of the states and are selected as

$$\begin{aligned}L_u^+ = \max\Bigg\{0,\, -u_{min} + a_\epsilon\,({E'_q}^* - L_\tau) - b_\epsilon\cos\delta - e_f\\ + k_\tau\left(1 - \frac{\mathrm{sat}^2(\omega-\omega^*)}{L_\tau^2}\right)\dot{\omega}\Bigg\},\end{aligned} \tag{25}$$

$$\begin{aligned}L_u^- = \max\Bigg\{0,\, u_{max} - a_\epsilon\,({E'_q}^* + L_\tau) + b_\epsilon\cos\delta + e_f\\ - k_\tau\left(1 - \frac{\mathrm{sat}^2(\omega-\omega^*)}{L_\tau^2}\right)\dot{\omega}\Bigg\}.\end{aligned} \tag{26}$$

We emphasize that, locally around the closed-loop operating equilibrium, both L_u^+ and L_u^- are positive. In addition, both L_u^+ and L_u^- can be made globally bounded by a proper selection of the slope constant k_τ.

3.1 Stability Analysis

To analyze the stability properties of the operating equilibrium of the third order model controlled with (23), let $\varepsilon = E'_q - \tilde{E}'_q$ indicate the difference between the state E'_q and its desired state-dependent reference $\tilde{E}'_q$. With this definition, the closed-loop SMIB power system can be rewritten as

$$\dot{\delta} = \omega - \omega^*, \tag{27}$$

$$\dot{\omega} = -\frac{(D+T_e)}{2H}(\omega-\omega^*) + \frac{\omega^*}{2H}(P_m - T_e), \tag{28}$$

$$\dot{\varepsilon} = -a_\epsilon\,\varepsilon - \mathrm{Sat}(\varepsilon), \tag{29}$$

where the electrical torque output $T_e \in \mathbb{R}_{\ge 0}$ is expressed, in the new coordinates, as

$$\begin{aligned}T_e(\delta,\omega,\varepsilon) = a_\tau\Big({E'_q}^* + [\varepsilon + \mathrm{sat}(\omega-\omega^*)]\Big)^2\\ + b_\tau\sin\delta\,\Big({E'_q}^* + [\varepsilon + \mathrm{sat}(\omega-\omega^*)]\Big)\\ + c_\tau\sin 2\delta + d_\tau\cos\delta.\end{aligned} \tag{30}$$

Note that the operating equilibrium of the closed-loop system in the new coordinates is $x^* = [\delta^* \quad \omega^* \quad \varepsilon^*]^T$, with $\varepsilon^* = 0$. Let $D_\tau = (D+T_e)/(2H)$, and note that $D_\tau \in \mathbb{R}_{\ge 0}$. Then, (28) can be rewritten as

$$\begin{aligned}\dot{\omega} &= -D_\tau(\omega-\omega^*) + \frac{\omega^*}{2H}(P_m - T_e)\\ &= -D_\tau(\omega-\omega^*) - \gamma(\delta) - d\,\mathrm{sat}(\omega-\omega^*)\\ &\quad - \frac{\omega^* a_\tau}{2H}\varepsilon^2 - \frac{\omega^*}{2H}\big(2a_\tau {E'_q}^* + b_\tau\sin\delta\big)\varepsilon,\end{aligned} \tag{31}$$

where

$$\begin{aligned}\gamma(\delta) &= \frac{\omega^*}{2H}\Big(-P_m + a_\tau {E'_q}^{*2} + b_\tau\sin\delta\,{E'_q}^*\\ &\quad + c_\tau\sin 2\delta + d_\tau\cos\delta\Big),\\ d &= \frac{\omega^*}{2H}\Big(2a_\tau {E'_q}^* + a_\tau\,\mathrm{sat}(\omega-\omega^*) + 2a_\tau + b_\tau\sin\delta\Big).\end{aligned}$$

Consider now the energy-based[2] Lyapunov function candidate

$$V(\delta,\omega,\varepsilon) = \frac{1}{2}(\omega-\omega^*)^2 + \theta(\delta) + \frac{\kappa_\varepsilon}{2}\varepsilon^2 + \frac{\omega^* a_\tau}{2H}\,\delta\,\varepsilon^2, \tag{32}$$

where $\kappa_\varepsilon \in \mathbb{R}_{>0}$ is a sufficiently large scaling constant to be selected, and θ is defined as

$$\theta(\delta) = \int_{\delta^*}^{\delta}\gamma(\xi)\,d\xi + c, \tag{33}$$

with $c \in \mathbb{R}$ such that $\theta(\delta^*) = 0$.

Note that θ is locally positive definite around the operating equilibrium, as illustrated in Fig. 3. Recall that $\delta \in [0,\pi]$, thus the term $\delta\,\varepsilon^2$ is locally positive definite around the operating equilibrium. Therefore, the Lyapunov function candidate (32) is locally positive definite around the operating equilibrium.

Taking the time-derivative of V along the trajectories of the closed-loop system (27), (28), (29) and (30) yields

[2] The quadratic term in ω is related to the mechanical kinetic energy, while the terms in δ and ε are related to the electro-mechanical potential energy.

$$
\begin{aligned}
\dot{V} &= (\omega-\omega^*)\,\dot{\omega} + \frac{d\theta(\delta)}{d\delta}\,\dot{\delta} + \kappa_\varepsilon\,\varepsilon\,\dot{\varepsilon} \\
&\quad + \frac{\omega^* a_\tau}{2H}\,\varepsilon^2\,\dot{\delta} + \frac{\omega^* a_\tau}{H}\,\delta\,\varepsilon\,\dot{\varepsilon} \\
&= -D_\tau(\omega-\omega^*)^2 - d\,(\omega-\omega^*)\,\mathrm{sat}(\omega-\omega^*) \\
&\quad - \left(\kappa_\varepsilon + \frac{\omega^* a_\tau}{H}\,\delta\right)\left(a_\epsilon\varepsilon^2 + \varepsilon\,\mathrm{Sat}(\varepsilon)\right) \\
&\quad - \frac{\omega^*\left(2a_\tau E_q'^{\,*} + b_\tau\sin\delta\right)}{2H}\,\varepsilon\,(\omega-\omega^*) \\
&\le -D_\tau(\omega-\omega^*)^2 - d\,(\omega-\omega^*)\,\mathrm{sat}(\omega-\omega^*) \\
&\quad - \left(\kappa_\varepsilon + \frac{\omega^* a_\tau}{H}\,\delta\right) a_\epsilon\varepsilon^2 - \left(\kappa_\varepsilon + \frac{\omega^* a_\tau}{H}\,\delta\right)\varepsilon\,\mathrm{Sat}(\varepsilon) \\
&\quad + \frac{\omega^*\left(2a_\tau E_q'^{\,*} + b_\tau\sin\delta\right)}{4H\kappa_\omega}\,\varepsilon^2 + \frac{\kappa_\omega}{2}(\omega-\omega^*)^2 \\
&= -\left(D_\tau - \frac{\kappa_\omega}{2}\right)(\omega-\omega^*)^2 \\
&\quad - d\,(\omega-\omega^*)\,\mathrm{sat}(\omega-\omega^*) \\
&\quad - \left(\kappa_\varepsilon + \frac{\omega^* a_\tau}{H}\,\delta - \frac{\omega^*\left(2a_\tau E_q'^{\,*} + b_\tau\sin\delta\right)}{4H\kappa_\omega\,a_\epsilon}\right) a_\epsilon\varepsilon^2 \\
&\quad - \left(\kappa_\varepsilon + \frac{\omega^* a_\tau}{H}\,\delta\right)\varepsilon\,\mathrm{Sat}(\varepsilon). \qquad (34)
\end{aligned}
$$

Since κ_ε is sufficiently large, setting $\kappa_\omega = 1$ yields

$$
\begin{aligned}
-\left(D_\tau - \frac{\kappa_\omega}{2}\right)(\omega-\omega^*)^2 &\le 0 \\
-d\,(\omega-\omega^*)\,\mathrm{sat}(\omega-\omega^*) &\le 0 \\
-\left(\kappa_\varepsilon + \frac{\omega^* a_\tau}{H}\,\delta - \frac{\omega^*\left(2a_\tau E_q'^{\,*} + b_\tau\sin\delta\right)}{4H\kappa_\omega\,a_\epsilon}\right) a_\epsilon\varepsilon^2 &\le 0 \\
-\left(\kappa_\varepsilon + \frac{\omega^* a_\tau}{H}\,\delta\right)\varepsilon\,\mathrm{Sat}(\varepsilon) &\le 0.
\end{aligned}
$$

Hence, $\dot{V} \le 0$, from which we conclude local stability of the post-fault closed-loop operating equilibrium. Finally, a direct application of *LaSalle's invariance principle* shows that the post-fault closed-loop operating equilibrium is also attractive, hence it is locally asymptotically stable.

In summary, the bounded state feedback control law (23) is such that the post-fault closed-loop operating equilibrium is locally asymptotically stable, and $u_{min} \le u(t) \le u_{max}, \forall\, t \in \mathbb{R}_{\ge 0}$.

3.2 Direct Method for Transient Stability Assessment

To use the Lyapunov function (32) as an tool for transient stability analysis, consider the graph of the function θ illustrated in Fig. 3. Note that the function θ has a local maximizer, denoted by δ^s, which is one of the solutions of the equation

$$
\frac{d\theta(\delta)}{d\delta} = \gamma(\delta) = 0. \qquad (35)
$$

In particular, δ^s is the smallest of such solutions *to the right* of the operating equilibrium δ^*. Note that while δ^s is a local maximizer of θ, it is a saddle point for the Lyapunov function V.

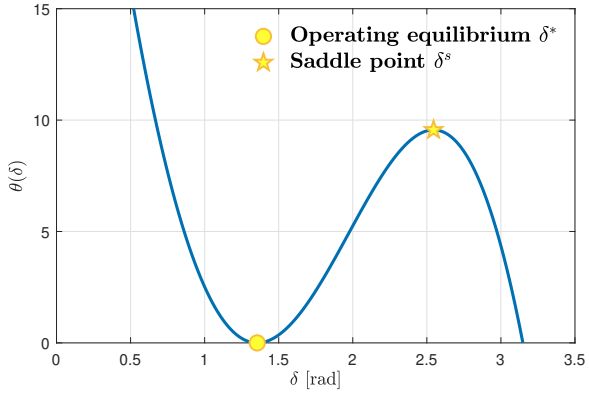

Fig. 3. Graph of the function θ in (33)

We now discuss how the energy-based Lyapunov function (32) can be used as an instrument for transient stability analysis. To this end, define the "critical" value

$$
V_c = V(\delta^s, \omega^*, \varepsilon^*), \qquad (36)
$$

and consider Algorithm 1.

Algorithm 1

Let $x(t_c) = x_c$ be the state of the SMIB power system at the instant the fault is cleared.
Calculate $V(x_c)$.
if $V(x_c) \le V_c$ **then**
the post-fault trajectory converges to its equilibrium,
else
no conclusion can be drawn, and TDS have to be conducted for the post-fault mode.
end

The idea of Algorithm 1 is as follows. The state trajectory at the instant the fault is cleared, *i.e.* x_c, is obtained through the simulation of the fault-on mode. Then, the value of the Lyapunov function at this state, *i.e.* $V(x_c)$, can be calculated. If $V(x_c) \le V_c$, indicating that the state x_c is inside the estimated region of attraction of the post-fault operating equilibrium, the post-fault trajectory converges to the post-fault operating equilibrium. Hence, the post-fault system is directly assessed to be stable. If instead $V(x_c) > V_c$, indicating that the state x_c is outside the estimated region of attraction of the post-fault operating equilibrium, the behaviour of the post-fault trajectory cannot be predicted because of the conservativeness of the estimation. In this case TDS have to be conducted for transient stability assessment.

4. CASE STUDY

The simulations in this case study are conducted based on the SMIB power system model shown in Fig. 1. Recall that the fault is assumed to occur at the location **F**. The control parameters and the saddle point in the case study are given in Table 3.

Table 3. Parameters in the case study

L_τ	k_τ	k_u	κ_ε	δ^s
0.2	0.108	20	240π	2.5454

4.1 Transient performance

To demonstrate the transient performance achievable with the proposed control approach, consider the following test scenario. The fault occurs at $t_f = 1s$. It is then cleared after a fault-on duration $\Delta t = 70\,ms$, *i.e.* it is cleared at the fault-clearing time $t_c = 1.070s$. Since the emphasis is on the stability of the post-fault mode, the designed bounded control law (23) is applied at the fault-clearing time, which results in the closed-loop post-fault mode, *i.e.* (27), (28) and (29).

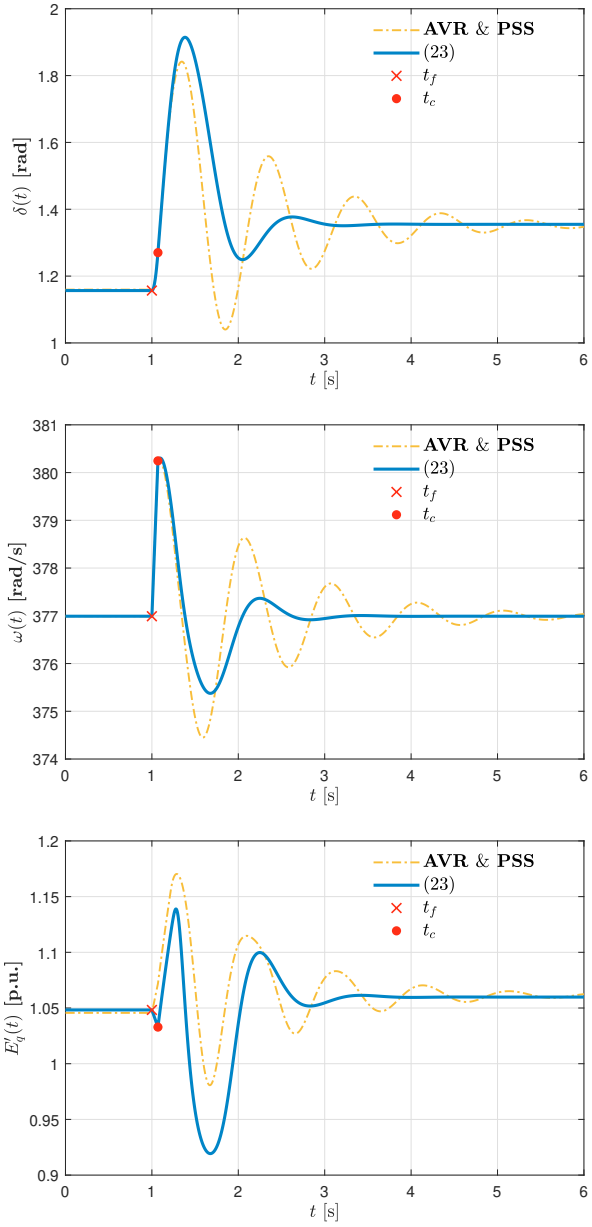

Fig. 4. Time histories of the SMIB power system states: rotor angle (top), rotational speed (middle) and induced voltage (bottom)

Fig. 4 illustrates the transient performances yielded by two control approaches, *i.e.* by the designed control law (23) and by the traditional AVR and PSS, respectively. It can be observed that the closed-loop transients yielded by the proposed control law have a faster convergence speed.

The control signals in the considered two approaches are displayed in Fig. 5. Since it is applied at the fault-clearing time, the proposed control is set to zero in the open-loop modes, *i.e.* in the pre-fault mode and the fault-on mode. Both control signals remain within the specified physical bounds. However, compared with the excitation control input provided by AVR and PSS, the designed bounded control input covers the whole range, indicating a higher utilization of the available control energy. Note that the use of the state-dependent gains L_u^+ and L_u^- in (25) and (26) is instrumental for this achievement.

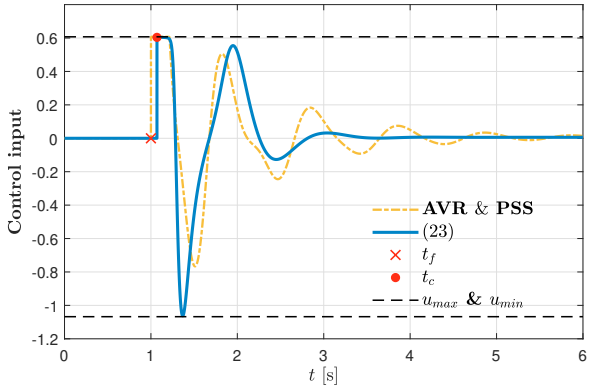

Fig. 5. Time histories of the control inputs

The state ε quantifies the tracking performance of the state E'_q against its desired state-dependent reference $\tilde{E}'_q$, the behaviour of which is displayed in Fig. 6. Since the control law (23) is applied at the fault-clearing time, the state ε stays zero in the open-loop modes. It jumps at the fault-clearing time and then converges exponentially to zero, consistently with (29).

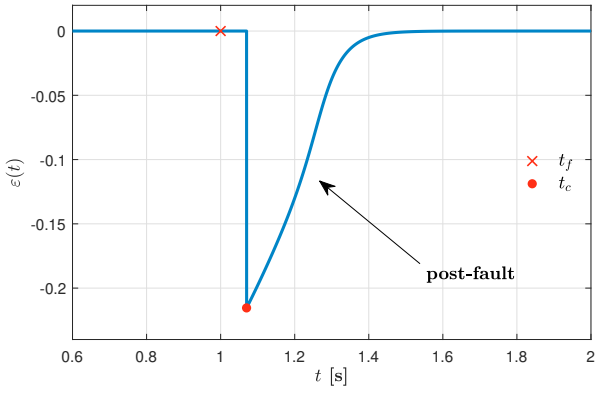

Fig. 6. Time history of the state ε

The Lyapunov function (32) serves as a monitor for the transient response with respect to the post-fault mode. Its time history in the considered transient stability case is shown in Fig. 7. Note that, after the fault-clearing instant, the Lyapunov function decreases monotonically to zero, consistent with the fact that the post-fault trajectory converges to the post-fault closed-loop operating equilibrium.

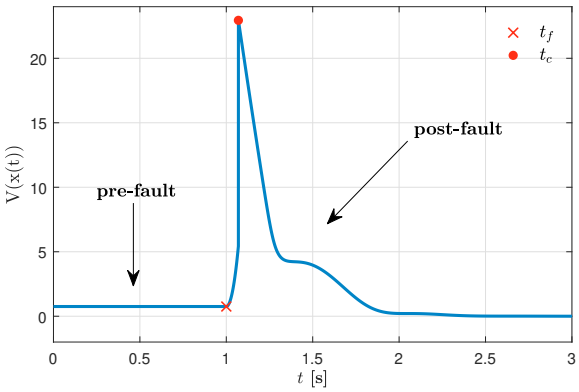

Fig. 7. Time history of the Lyapunov function V

4.2 Stability of the Post-fault Trajectories

To visualize the transient response of the post-fault closed-loop system, consider the level sets of the Lyapunov function projected into the δ-ω plane illustrated in Fig. 8. The (yellow) circle is the projection of the post-fault operating equilibrium, while the (yellow) pentagram is the projection of the saddle point. The region, enclosed by the solid curve containing the saddle point, represents the estimated region of attraction of the post-fault operating equilibrium.

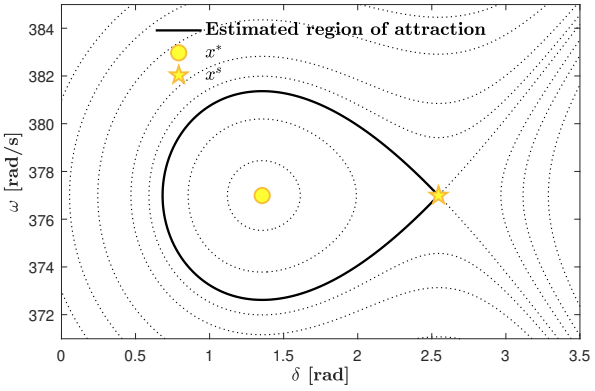

Fig. 8. Level sets and the estimated region of attraction of the post-fault operating equilibrium

To demonstrate the performance of the proposed direct method, consider the following test scenarios (recall that the fault occurs at $t_f = 1s$). Three cases with fault-on durations of $\Delta t_1 = 90\,ms$, $\Delta t_2 = 100\,ms$, and $\Delta t_3 = 105\,ms$, respectively, are considered. Then, the resulting state trajectories projected into the δ-ω plane are displayed in Fig. 9 and in Fig. 10, respectively. In each plot, the (red) cross represents the projection of the state at the time the fault occurs, while the (red) circle represents the projection of the state at the fault-clearing time, *i.e.* x_c.

If x_c is inside the estimated region of attraction of the post-fault equilibrium, described by the condition $V(x_c) \leq V_c$, the post-fault trajectory converges to the operating equilibrium. This is the case with $\Delta t_1 = 90\,ms$. Note that, for any fault-on duration shorter than Δt_1, the post-fault trajectory converges to the post-fault operating equilibrium. In conclusion, the post-fault SMIB power system controlled with (23) is directly assessed to be stable given that the fault-on duration is shorter than Δt_1.

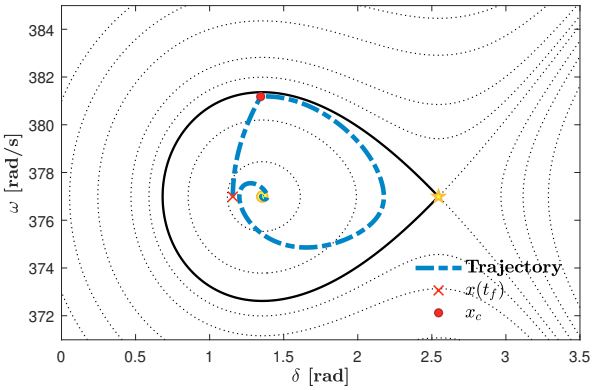

Fig. 9. Projection of the state trajectory in the case with $\Delta t_1 = 90\,ms$

If x_c is outside the estimated region of attraction of the post-fault equilibrium, that is the condition $V(x_c) > V_c$ holds, no conclusion can be drawn on the behaviour of the post-fault trajectory. This can either converge to the post-fault operating equilibrium or diverge, as illustrated in Fig. 10. In such cases, TDS for the post-fault trajectories should be used, as an auxiliary tool, to assess the transient stability.

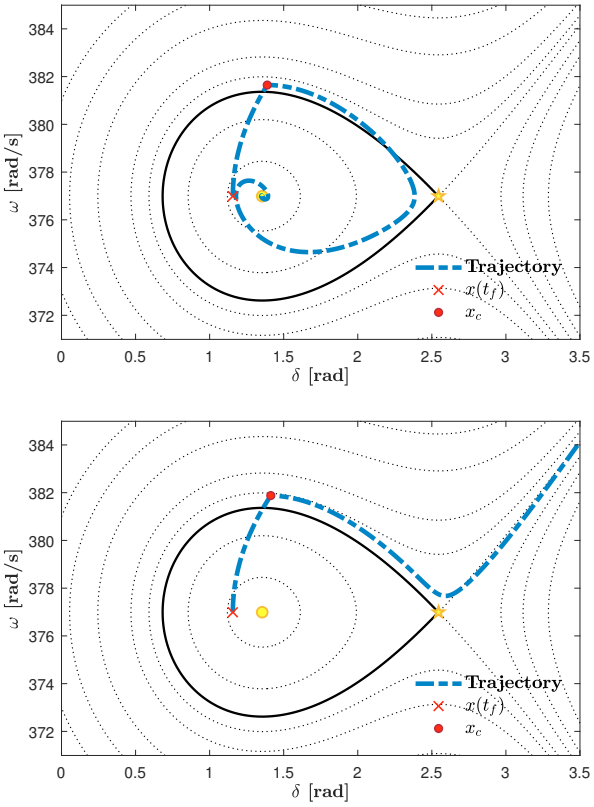

Fig. 10. Projections of the state trajectories in the cases with $\Delta t_2 = 100\,ms$ (top) and $\Delta t_3 = 105\,ms$ (bottom)

Table 4 summarizes the conclusion for the considered test scenarios.

Table 4. Transient stability assessment results

Δt	$V(x_c) \leq V_c$	Assessment
$90\,ms$	Yes	Direct assessment: Stable
$100\,ms$	No	Conduct TDS: Stable
$105\,ms$	No	Conduct TDS: Unstable

Note, in particular, that in the case with fault-on duration of $\Delta t_2 = 100\,ms$, although the state at the fault-clearing time x_c is outside the estimated region of attraction of the post-fault operating equilibrium, the post-fault trajectory converges to the post-fault equilibrium and is assessed to be stable. This indicates that the estimated region of attraction, the projection of which on the δ-ω plane is illustrated in Fig. 8, is a subset of the actual region of attraction of the post-fault operating equilibrium.

5. CONCLUSION AND FUTURE WORK

This paper has proposed a new bounded state feedback control law with independently adjustable upper and lower bounds. On the basis of the proposed control law, an energy-based Lyapunov function for the third order model of a closed-loop SMIB power system is proposed. The Lyapunov function allows assessing local stability of the closed-loop operating equilibrium, and serves as a monitor for the transient performance of the post-fault trajectory. Finally, by comparing the value of the proposed Lyapunov function at the state at the fault-clearing time against a critical value, we can construct an indicator for the stability assessment of the post-fault mode.

One direction for future work is to extend the proposed method to more detailed models of synchronous generators and to multi-machine power systems. Finally, one could also improve the proposed bounded control law by removing its dependence on non-measurable states.

REFERENCES

Bretas, N.G. and Alberto, L.F. (2003). Lyapunov function for power systems with transfer conductances: extension of the invariance principle. *IEEE Transactions on Power Systems*, 18(2), 769–777.

Chaudhuri, N., Chaudhuri, B., Majumder, R., and Yazdani, A. (2014). *Multi-terminal direct-current grids*. Wiley Online Library.

Chiang, H.D. (2011). *Direct methods for stability analysis of electric power systems: theoretical foundation, BCU methodologies, and applications*. John Wiley & Sons.

Ghandhari, M., Andersson, G., and Hiskens, I.A. (2001). Control lyapunov functions for controllable series devices. *IEEE Transactions on Power Systems*, 16(4), 689–694.

Guo, Y., Hill, D.J., and Wang, Y. (2001). Global transient stability and voltage regulation for power systems. *IEEE Transactions on Power Systems*, 16(4), 678–688.

Hatziargyriou, N., Milanovic, J., Rahmann, C., Ajjarapu, V., Canizares, C., Erlich, I., Hill, D., Hiskens, I., Kamwa, I., Pal, B., et al. (2020). Definition and classification of power system stability — revisited & extended. *IEEE Transactions on Power Systems*.

Jiang, N. and Chiang, H.D. (2015). A two-time scale dynamic correction method for fifth-order generator model undergoing large disturbances. *IEEE Transactions on Power Systems*, 31(5), 3616–3623.

Kundur, P., Balu, N.J., and Lauby, M.G. (1994). *Power system stability and control*, volume 7. McGraw-hill New York.

Liberzon, D. (2003). *Switching in systems and control*. Springer Science & Business Media.

Ortega, R., Galaz, M., Astolfi, A., Sun, Y., and Shen, T. (2005). Transient stabilization of multimachine power systems with nontrivial transfer conductances. *IEEE Transactions on Automatic Control*, 50(1), 60–75.

Pai, M. and Sauer, P.W. (1989). Stability analysis of power systems by Lyapunov's direct method. *IEEE Control Systems Magazine*, 9(1), 23–27.

Sauer, P.W. and Pai, M.A. (1998). *Power system dynamics and stability*, volume 101. Wiley Online Library.

Verrelli, C.M., Marino, R., Tomei, P., and Damm, G. (2021). Nonlinear robust coordinated PSS-AVR control for a synchronous generator connected to an infinite bus. *IEEE Transactions on Automatic Control*.

Yan, J., Liu, C.C., and Vaidya, U. (2011). PMU-based monitoring of rotor angle dynamics. *IEEE Transactions on Power Systems*, 26(4), 2125–2133.